Prospects for the Detection of Electronic Preturbulence in Graphene

A. Gabbana,[1,2] M. Polini,[3] S. Succi,[4,5] R. Tripiccione,[1] and F. M. D. Pellegrino[6,7]
[1]*Università di Ferrara and INFN-Ferrara, I-44122 Ferrara, Italy*
[2]*Bergische Universität Wuppertal, D-42119 Wuppertal, Germany*
[3]*Istituto Italiano di Tecnologia, Graphene Labs, Via Morego 30, I-16163 Genova, Italy*
[4]*Center for Life Nano Science at La Sapienza, Italian Institute of Technology, Viale Regina Elena 295, I-00161 Roma, Italy*
[5]*Istituto Applicazioni del Calcolo, National Research Council of Italy, Via dei Taurini 19, I-00185 Roma, Italy*
[6]*Dipartimento di Fisica e Astronomia, Università di Catania, Via S. Sofia 64, I-95123 Catania, Italy*
[7]*INFN, Sezione Catania, I-95123 Catania, Italy*

(Received 7 August 2018; published 5 December 2018)

Based on extensive numerical simulations, accounting for electrostatic interactions and dissipative electron-phonon scattering, we propose experimentally realizable geometries capable of sustaining electronic preturbulence in graphene samples. In particular, preturbulence is predicted to occur at experimentally attainable values of the Reynolds number between 10 and 50, over a broad spectrum of frequencies between 10 and 100 GHz.

DOI: 10.1103/PhysRevLett.121.236602

Introduction.—Hydrodynamic theory [1,2] has proven very successful in describing a large variety of physical systems, across a broad range of scales, temperature, and density regimes. The ultimate reason of this success is "universality," namely, the insensitivity of the hydrodynamic description to the details of the underlying microscopic physics, as long as such details do not spoil the basic mass, momentum, and energy conservation laws, which underpin the emergence of hydrodynamic behavior.

Under such conditions, at "sufficiently large" scales ("large" meaning much larger than the typical microscopic interaction length), the specific details of the interactions among the constituent particles do not affect the structure of the hydrodynamic equations but only the actual values of the transport coefficients controlling dissipative effects, such as the shear and bulk viscosity, as well as the thermal conductivity.

Even if electrons roaming in a crystal can lose energy and momentum towards impurities and the lattice, transport in systems where the mean free path for electron-electron collisions is the shortest length scale of the problem can also be described by hydrodynamic theory and the Navier-Stokes equations [3–34]. Interestingly, phonon transport is also expected to display hydrodynamic features [35,36].

Recent experiments carried out in high-quality encapsulated graphene sheets [37–40] and GaAs quantum wells [41] have demonstrated unique qualitative features of hydrodynamic electron transport, namely, a negative quasilocal resistance [37,39–41] and superballistic electron flow [38], providing, for the first time, the ability to directly measure the dissipative shear viscosity η of a two-dimensional (2D) electron system. A different experiment [42] has shown that, near charge neutrality, electron-electron interactions in graphene are strong enough to yield substantial violations of the Wiedemann-Franz law. Evidence of hydrodynamic transport has also been reported in quasi-2D channels of palladium cobaltate [43]. For a recent review, see Ref. [44].

Given this context, it is natural to investigate conditions under which nonlinear terms of the Navier-Stokes equations, which have proven unnecessary so far to explain experimental results [37–43], may become relevant.

In this Letter, we identify a range of geometrical and physical parameters, in which electronic preturbulence can be triggered and sustained in experimentally realizable graphene samples, provided a substantial reduction of electron-phonon scattering is achieved in future experiments. In this context, preturbulence refers to a regime prior to the onset of chaos, where periodic oscillations of the velocity field can be observed, without necessarily exhibiting chaotic behavior [45]. To this purpose, we performed extensive numerical simulations *taking into account* electrostatic interactions and electron-phonon scattering. In particular, we propose suitable geometries for which preturbulence (i) occurs at experimentally achievable values of the Reynolds number and (ii) exhibits temporal fluctuations of the electrical potential over a spectrum of frequencies between 10 and 100 GHz.

Kinetic description and Boltzmann equation.—The direct solution of the Navier-Stokes equations presents a numerically challenging task. In the past decades, it has become apparent that a broad class of complex flows can be addressed by solving suitably simplified lattice versions of Boltzmann's kinetic equation [46] (for details, see Supplemental Material [47]).

For the specific 2D electron system of interest in this work, Boltzmann's kinetic equation reads as follows:

$$\left(\frac{\partial}{\partial t}+\frac{\boldsymbol{p}}{m}\cdot\nabla+\boldsymbol{F}\cdot\frac{\partial}{\partial \boldsymbol{p}}\right)f=\Omega, \tag{1}$$

where $f(\boldsymbol{r},\boldsymbol{p},t)$ is the one-particle distribution function expressing the average number of particles in a small element of phase space centered at position $\boldsymbol{r}$ with momentum $\boldsymbol{p}$ at time t. In the above, m is a suitable effective mass, $\boldsymbol{F}$ is the sum of all external forces acting on the system, and Ω is the collision operator, commonly replaced by a relaxation term towards local equilibrium [61].

It is well known that hydrodynamics emerges from Eq. (1) in the limit of small Knudsen numbers [62], leading to the continuity, Navier-Stokes, and energy-conservation equations. Microscopic details are reflected by the transport coefficients.

The bulk viscosity ζ is negligibly small for electrons in graphene [22], and, while the lattice Boltzmann equation usually features a nonzero value, it has no effect on the physics discussed here, since the flow is nearly incompressible. The shear viscosity η, on the other hand, plays a crucial role [37–40], and, consequently, it is taken in full account.

For the specific case of 2D electrons in doped graphene, the total force is taken in the following form:

$$\boldsymbol{F}=e\nabla\varphi(\boldsymbol{r},t)-\frac{n(\boldsymbol{r},t)\boldsymbol{v}(\boldsymbol{r},t)}{\tau_D}. \tag{2}$$

The first term on the right-hand side describes electrical forces acting on a fluid element, $-e$ being the elementary charge and $\varphi(\boldsymbol{r},t)$ the electrical potential in the 2D plane where electrons move. The second term describes forces that dissipate electron momentum, i.e., due to collisions between electrons and external agents, such as acoustic phonons in graphene. These are parametrized as an external friction, with a single timescale, i.e., the Drude-like scattering time τ_D. This simple parametrization has proven extremely successful in describing experiments in the linear-response regime [37–41].

Following Ref. [16], we utilize the local capacitance approximation in which the electrical potential is approximated as $\varphi(\boldsymbol{r},t)\approx -e\delta n(\boldsymbol{r},t)/C_g$, where C_g is the geometrical capacitance of the graphene device of interest and $\delta n(\boldsymbol{r},t)=n(\boldsymbol{r},t)-\bar{n}$, $\bar{n}$ being the uniform value of the electron density set by a nearby metallic gate. Using a similar local approximation for the gradient of the pressure [63], i.e., $\nabla P\approx(\partial P/\partial n)_{n(\boldsymbol{r},t)\to\bar{n}}\nabla\delta n(\boldsymbol{r},t)$, we can define the electrochemical potential as $\Phi(\boldsymbol{r},t)\equiv -e\delta n(\boldsymbol{r},t)(C_g^{-1}+C_Q^{-1})$, $C_Q=2\bar{n}e^2/E_F$ being the so-called quantum capacitance [63] and $E_F=\hbar v_F\sqrt{\pi\bar{n}}$ the Fermi energy in single-layer graphene (SLG). Finally, $v_F\simeq 10^6$ m/s is the Fermi velocity of massless Dirac fermions in SLG. With reference to Eq. (1), we use the usual effective mass $m=E_F/v_F^2$ for SLG.

Our numerical results are based on extensive numerical simulations of the geometry shown in Fig. 1(a), which can be easily realized experimentally with current technology, and for a large set of values of the relevant physical parameters (see Table I). All cases considered in this work fall in a regime of very small Mach number Ma, in which compressibility effects can safely be neglected. The Mach number is defined as the ratio between the plasma-wave velocity v_{PW} and the fluid velocity of the electron fluid, with $v_{\mathrm{PW}}=\sqrt{e^2\bar{n}v_F^2/(CE_F)}$, where $C^{-1}=C_g^{-1}+C_Q^{-1}$. For the device geometry shown in Fig. 1(a) and the parameters used in all our simulations, $\mathrm{Ma}\ll 1$. [This has been explicitly verified *a posteriori* for all cases. For example, for the simulations corresponding to Figs. 1(b)–1(d), we have $\mathrm{Ma}\approx 0.0015$, 0.08, and, 0.12, respectively.] A small value of Ma in turn implies the quasi-incompressibility of the electron fluid. As mentioned earlier on, in this regime we have resorted to a lattice Boltzmann (LB) approach [64], which, among others, offers the advantage of a comparatively simple handling of non-idealized geometrical boundary conditions. In this work, we use a nonrelativistic LB scheme, since relativistic approaches [65–67] are appropriate only very close to the charge neutrality point, where charge and energy flows

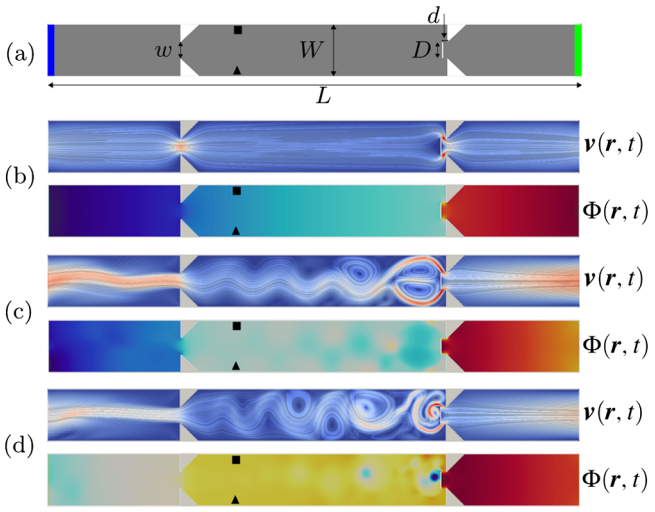

FIG. 1. Preturbulence in high-quality graphene. (a) Geometrical details of the setup analyzed in this work. Two graphene leads of width $W=1$ μm are attached via "funnels" to a central area. Current is injected through an orifice of width $w=0.32$ μm with an obstacle of length $D=0.3$ μm placed at a lateral distance $d=0.1$ μm from the orifice. (b)–(d) Snapshots of simulations for several values of the injected current. (b) Velocity field $\boldsymbol{v}(\boldsymbol{r},t)$ (top) and electrochemical potential $\Phi(\boldsymbol{r},t)$ (bottom) for an injected current $I=10^{-6}$ A. (c) The same as in (b) but for an injected current $I=5\times 10^{-4}$A. (d) The same as in (b) and (c) but for $I=10^{-3}$ A. Data in (b)–(d) have been obtained by setting $\nu=4\times 10^{-4}$ m^2/s, $\tau_D=50$ ps, and $C_g/e^2=1.52\times 10^{35}$ J^{-1} m^{-2} (see the text for definitions of all quantities).

TABLE I. Typical values of physical parameters of state-of-the-art experiments compared with those used in our simulations. Refer to Fig. 1(a) for the definition of L and W. All other parameters are defined in the main text.

	Typical experiments	This work
L	5–30 [μm]	10 [μm]
W	1–5 [μm]	1 [μm]
$\bar{n}$	$0.5\text{–}4 \times 10^{12}$ [cm^{-2}]	2×10^{12} [cm^{-2}]
I	$10^{-3} - 1$ [mA]	$10^{-3} - 1$ [mA]
ν	0.01–0.1 [m^2/s]	10^{-4}–10^{-3} [m^2/s]
τ_D	1–5 [ps]	1–400 [ps]
C_g/e^2	3.03×10^{34} [J^{-1} m^{-2}]	3.03×10^{35} [J^{-1} m^{-2}]

are coupled [44]. Technical details on this numerical approach are reported in Ref. [47].

Numerical results.—We consider a geometry close to the one used in recent experimental work [38], which made use of a constriction to emphasize a clear crossover from the ballistic Sharvin regime to the hydrodynamic regime as a function of the temperature. Such a geometry is sketched in Fig. 1(a), with the addition of a thin linear obstacle, placed in front of the constriction, with the intent of triggering preturbulent regimes at low Reynolds numbers.

Figure 1 qualitatively summarizes our finding. For appropriate values of the transport parameters [low enough kinematic viscosity $\nu = \eta/(nm)$ and large enough τ_D], a laminar behavior is found for low values of the current [10^{-3} mA, Fig. 1(b)] injected in the sample. As the value of the injected current is increased [0.5–1.0 mA, Figs. 1(c) and 1(d), and, correspondingly, the typical fluid element velocity increases], the onset of a preturbulent regime takes place (identified with a procedure described later in the text).

Present-day experiments cannot map the fluid velocity everywhere in the sample but typically can only measure the electrochemical potential (also mapped in Fig. 1) at selected sites on the boundaries. The expected result of such measurements is shown in Fig. 2(a), displaying the electrochemical potential difference between locations corresponding to the black square and triangle in Fig. 1(a); here again, we appreciate a clear change from a constant to a periodic, to a more irregular trend, which is best analyzed in the frequency domain; see Fig. 2(b). The present simulations cover a wide region in the $\nu - \tau_D$ plane. Results are collected in Fig. 3, showing the smallest value of τ_D as a function of ν, for which a crossover to an observable preturbulent regime occurs, denoted by the symbol τ_D^*. Here and throughout, we shall refer to "crossover" as a generic term, since investigating the possibility of critical behavior is beyond the scope of the present work.

Points in Fig. 3 refer to experimentally achievable values of the injected current of the order of $\approx$1 mA. They have been determined using the onset of a transverse current along the middle section of the device as a discriminating factor; the upper end of these points are simulations for which the root mean square of the transverse current exceeds 1% of the magnitude of the injected current (more details in Supplemental Material [47]).

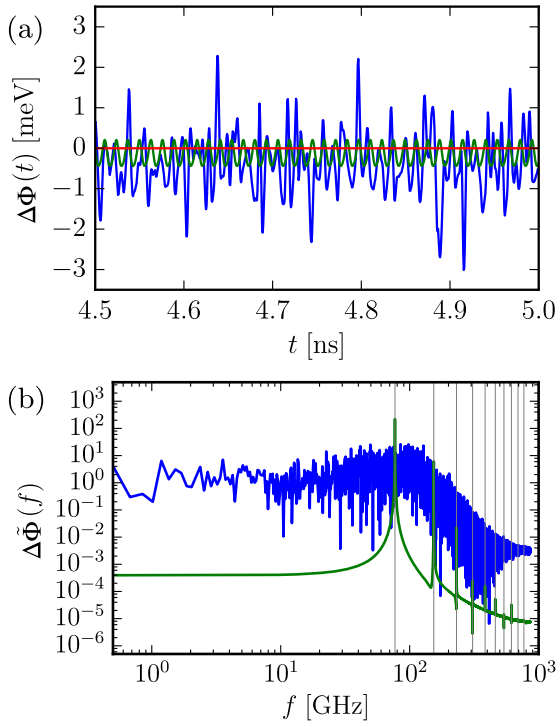

FIG. 2. (a) Time evolution of the electrochemical potential difference $\Delta\Phi = \Phi(\bar{r}, t) - \Phi(\bar{r}', t)$, with $\bar{r} = (3\ \mu\text{m}, 0.1\ \mu\text{m})$ and $\bar{r}' = (3\ \mu\text{m}, 0.9\ \mu\text{m})$. These two points have been marked in Fig. 1(a) by a triangle ($\bar{r}$) and a square ($\bar{r}'$). Numerical results shown is this figure have been taken from simulations using $\nu = 4 \times 10^{-4}$ m^2/s, $\tau_D = 50$ ps, $C_g/e^2 = 1.52 \times 10^{35}$ J^{-1} m^{-2}, and the following values of the injected current: $I = 10^{-6}$A (red), $I = 5 \times 10^{-4}$A (green), and $I = 10^{-3}$A (blue). (b) Power spectrum of the signals shown in (a). The gray vertical lines represent the first ten harmonics of the dominant frequency of the periodic signal obtained from the simulation at injected current $I = 5 \times 10^{-4}$A.

Recent works [37,38] have reported direct experimental measurements of the kinematic viscosity ν of the 2D electron system in graphene, which are on the order of $\nu \lesssim 0.1$ m^2/s. As far as electron-phonon interactions are concerned, state-of-the-art experiments in graphene encapsulated between hexagonal boron nitride (hBN) crystals display τ_D ranging between 1 and 2 ps in the temperature range 70–300 K, where hydrodynamic behavior is strongest. Inspection of Fig. 3 may therefore convey disappointing news: For values of the parameters currently achieved in experiments, no preturbulent behavior can be detected. The mitigating observation is that substantial, but not inconceivable, improvements of the transport

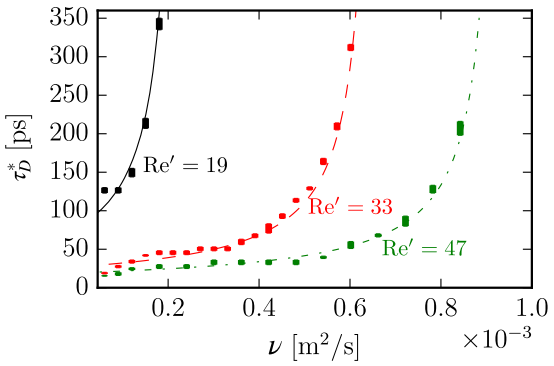

FIG. 3. Value of the Drude-like scattering time τ_D^* as a function of the kinematic viscosity ν, for which the crossover from a laminar to a preturbulent regime is observed. Thick vertical bars represent results of numerical simulations (refer to Ref. [47] for details on how these intervals are established), with the following values of the injected current: $I = 10^{-4}$ A (black), $I = 5 \times 10^{-4}$ A (red), and $I = 10^{-3}$ A (green). Lines represent iso-Reynolds curves, where Re′ as in Eq. (3) is used in the definition of a Reynolds number that includes extrinsic dissipation due to τ_D and ℓ is a fitting parameter. Lines represents fits to the numerical data: $I = 10^{-4}$ A (solid black line), $I = 5 \times 10^{-4}$ A (red dashed line), and $I = 10^{-3}$ A (green dash-dotted line). Refer to Fig. 1(a) for details on the geometry used in the simulations. Numerical data in this figure have been obtained by setting $C_g/e^2 = 3.03 \times 10^{35}$ J^{-1} m^{-2}.

parameters may eventually turn the picture for good. For example, the viscosity of the electron liquid at elevated injection currents, as those needed to achieve the preturbulent regime, is expected to be much smaller than that in the linear-response regime, due to Joule heating [68], which notably increases the electron temperature above the lattice temperature. Moreover, recent material science advances [69] have enabled much larger values of τ_D than those measured in hBN-encapsulated graphene. Such large values of τ_D can be obtained by using different encapsulating materials, such as WSe_2, which are currently believed to quench scattering of electrons against acoustic phonons in graphene [69].

A further encouraging result is that the frequency distribution of the electrochemical potential falls within a measurable regime, if only with suitably designed experiments.

From a purely fluid-dynamics point of view, it may be interesting to characterize the crossover line clearly shown in Fig. 3 in terms of an appropriate figure of merit. To this purpose, we develop a simplified model, whose starting point is the role played by the Reynolds number as an indicator of turbulence. In the present case, the turbulence-suppressing effect of the dissipative term in the Navier-Stokes equation is augmented by electron-phonon scattering. On purely dimensional grounds, it proves expedient to introduce a modified Reynolds number Re′, incorporating the effect of electron-phonon dissipation, namely,

$$\mathrm{Re}' = \frac{|\boldsymbol{v}|\ell}{\nu + \frac{\ell^2}{\tau_D}}, \tag{3}$$

with $|\boldsymbol{v}|$ a typical fluid-element velocity and ℓ a typical length scale for the system at hand.

This very simple model proves adequate to characterize the actual behavior of the system. Lines in Fig. 3 are level lines for Re′, which capture the trend of the different data sets. In Eq. (3), we use the inlet velocity and obtain $\ell = 0.135$ μm through a linear fit. Such a value turns out to be pretty close to the typical geometrical features of the simulated layout.

We obtain the following estimates for the values of the modified Reynolds numbers at the crossover: $\mathrm{Re}' \sim 19$ for $I = 10^{-4}$A, $\mathrm{Re}' \sim 33$ for $I = 5 \times 10^{-4}$ A, and $\mathrm{Re}' \sim 47$ for $I = 10^{-3}$ A.

We do not wish to attach any deep meaning to this parametrization but simply note that it discloses a simple theoretical interpretation of the numerical results.

The Strouhal number $\mathrm{St} = f\ell/|\boldsymbol{v}|$, where f is the shedding frequency, might also be considered in order to identify the crossover line. This is suggested by a preliminary analysis showing that at fixed Re′ the value of St is remarkably stable as we vary ν and τ_D along each crossover line. For instance, at $\mathrm{Re}' = 47$ we have $\mathrm{St} = 0.028 \pm 0.001$, which is comparable with previous findings [13]. The corresponding frequencies f increase monotonically with Re′ and are in the range 20–80 GHz. We plan to further analyze the role of St in future works.

Closing remarks.—In summary, based on extensive numerical simulations, accounting for electrostatic and dissipative effects due to electron-phonon scattering in experimentally realistic geometries, we have identified parameter regimes under which electronic preturbulence may eventually be detected by future experiments. To this purpose, such experiments should operate at lower levels of electron-phonon scattering (i.e., $\tau_D \sim 20$–50 ps) than those that can be achieved in hBN-encapsulated graphene, which is possible by using different encapsulating materials [69]. As a typical signature of electronic preturbulence, we predict electrical potential fluctuations in the frequency range between 10 and 100 GHz, which should be detectable by suitably designed experiments.

We emphasize that the placement of a thin plate across the mainstream electron flow in a constricted channel proves instrumental in lowering the Reynolds number at which preturbulence occurs. Further optimization may result from a concerted effort between future numerical and experimental investigations.

We thank Andre Geim and Iacopo Torre for useful discussions. We thank an anonymous referee for suggesting to consider the Strouhal number to further characterize the flow. A. G. has been supported by the European Union's Horizon 2020 research and innovation program under the

Marie Sklodowska-Curie Grant Agreement No. 642069. M. P. is supported by the European Union's Horizon 2020 research and innovation program under Grant Agreement No. 785219—GrapheneCore2. S. S. acknowledges funding from the European Research Council under the European Union's Horizon 2020 framework program (No. P/2014-2020)/ERC Grant Agreement No. 739964 (COPMAT). The numerical work has been performed on the COKA computing cluster at Università di Ferrara.

[1] L. D. Landau and E. M. Lifshitz, *Course of Theoretical Physics: Fluid Mechanics* (Pergamon, New York, 1987).
[2] G. Falkovich, *Fluid Mechanics* (Cambridge University Press, Cambridge, England, 2011).
[3] R. N. Gurzhi, Sov. Phys. Usp. **11**, 255 (1968).
[4] M. Dyakonov and M. Shur, Phys. Rev. Lett. **71**, 2465 (1993).
[5] M. I. Dyakonov and M. S. Shur, Phys. Rev. B **51**, 14341 (1995).
[6] M. Dyakonov and M. Shur, IEEE Trans. Electron Devices **43**, 380 (1996).
[7] S. Conti and G. Vignale, Phys. Rev. B **60**, 7966 (1999).
[8] A. O. Govorov and J. J. Heremans, Phys. Rev. Lett. **92**, 026803 (2004).
[9] M. Müller and S. Sachdev, Phys. Rev. B **78**, 115419 (2008).
[10] L. Fritz, J. Schmalian, M. Müller, and S. Sachdev, Phys. Rev. B **78**, 085416 (2008).
[11] M. Müller, J. Schmalian, and L. Fritz, Phys. Rev. Lett. **103**, 025301 (2009).
[12] R. Bistritzer and A. H. MacDonald, Phys. Rev. B **80**, 085109 (2009).
[13] M. Mendoza, H. J. Herrmann, and S. Succi, Phys. Rev. Lett. **106**, 156601 (2011).
[14] D. Svintsov, V. Vyurkov, S. Yurchenko, T. Otsuji, and V. Ryzhii, J. Appl. Phys. **111**, 083715 (2012).
[15] M. Mendoza, H. J. Herrmann, and S. Succi, Sci. Rep. **3**, 1052 (2013).
[16] A. Tomadin and M. Polini, Phys. Rev. B **88**, 205426 (2013).
[17] B. N. Narozhny, I. V. Gornyi, M. Titov, M. Schütt, and A. D. Mirlin, Phys. Rev. B **91**, 035414 (2015).
[18] U. Briskot, M. Schütt, I. V. Gornyi, M. Titov, B. N. Narozhny, and A. D. Mirlin, Phys. Rev. B **92**, 115426 (2015).
[19] I. Torre, A. Tomadin, A. K. Geim, and M. Polini, Phys. Rev. B **92**, 165433 (2015).
[20] L. Levitov and G. Falkovich, Nat. Phys. **12**, 672 (2016).
[21] F. M. D. Pellegrino, I. Torre, A. K. Geim, and M. Polini, Phys. Rev. B **94**, 155414 (2016).
[22] A. Principi, G. Vignale, M. Carrega, and M. Polini, Phys. Rev. B **93**, 125410 (2016).
[23] A. Lucas, J. Crossno, K. C. Fong, P. Kim, and S. Sachdev, Phys. Rev. B **93**, 075426 (2016).
[24] P. S. Alekseev, Phys. Rev. Lett. **117**, 166601 (2016).
[25] G. Falkovich and L. Levitov, Phys. Rev. Lett. **119**, 066601 (2017).
[26] H. Guo, E. Ilsevena, G. Falkovich, and L. S. Levitov, Proc. Natl. Acad. Sci. U.S.A. **114**, 3068 (2017).
[27] F. M. D. Pellegrino, I. Torre, and M. Polini, Phys. Rev. B **96**, 195401 (2017).
[28] A. Levchenko, H. Y. Xie, and A. V. Andreev, Phys. Rev. B **95**, 121301(R) (2017).
[29] T. Scaffidi, N. Nandi, B. Schmidt, A. P. Mackenzie, and J. E. Moore, Phys. Rev. Lett. **118**, 226601 (2017).
[30] L. V. Delacretaz and A. Gromov, Phys. Rev. Lett. **119**, 226602 (2017).
[31] D. Y. H. Ho, I. Yudhistira, N. Chakraborty, and S. Adam, Phys. Rev. B **97**, 121404(R) (2018).
[32] A. S. Petrov and D. Svintsov, arXiv:1802.03994.
[33] A. Lucas and S. D. Sarma, Phys. Rev. B **97**, 245128 (2018).
[34] A. Lucas and S. D. Sarma, Phys. Rev. B **97**, 115449 (2018).
[35] G. Fugallo, A. Cepellotti, L. Paulatto, M. Lazzeri, N. Marzari, and F. Mauri, Nano Lett. **14**, 6109 (2014).
[36] A. Cepellotti, G. Fugallo, L. Paulatto, M. Lazzeri, F. Mauri, and N. Marzari, Nat. Commun. **6**, 6400 (2015).
[37] D. Bandurin, I. Torre, R. K. Kumar, M. B. Shalom, A. Tomadin, A. Principi, G. H. Auton, E. Khestanova, K. S. NovoseIov, I. V. Grigorieva, L. A. Ponomarenko, A. K. Geim, and M. Polini, Science **351**, 1055 (2016).
[38] R. K. Kumar, D. A. Bandurin, F. M. D. Pellegrino, Y. Cao, A. Principi, H. Guo, G. H. Auton, M. B. Shalom, L. A. Ponomarenko, G. Falkovich, I. V. Grigorieva, L. S. Levitov, M. Polini, and A. K. Geim, Nat. Phys. **13**, 1182 (2017).
[39] A. I. Berdyugin, S. G. Xu, F. M. D. Pellegrino, R. K. Kumar, A. Principi, I. Torre, M. B. Shalom, T. Taniguchi, K. Watanabe, I. V. Grigorieva, M. Polini, A. K. Geim, and D. A. Bandurin, arXiv:1806.01606.
[40] D. A. Bandurin, A. V. Shytov, G. Falkovich, R. K. Kumar, M. B. Shalom, I. V. Grigorieva, A. K. Geim, and L. S. Levitov, arXiv:1806.03231.
[41] B. A. Braem, F. M. D. Pellegrino, A. Principi, M. Röösli, S. Hennel, J. V. Koski, M. Berl, W. Dietsche, W. Wegscheider, M. Polini, T. Ihn, and K. Ensslin, arXiv:1807.03177.
[42] J. Crossno, J. K. Shi, K. Wang, X. Liu, A. Harzheim, A. Lucas, S. Sachdev, P. Kim, T. Taniguchi, K. Watanabe, T. A. Ohki, and K. C. Fong, Science **351**, 1058 (2016).
[43] P. J. W. Moll, P. Kushwaha, N. Nandi, B. Schmidt, and A. P. Mackenzie, Science **351**, 1061 (2016).
[44] A. Lucas and K. C. Fong, J. Phys. Condens. Matter **30**, 053001 (2018).
[45] J. K. Kaplan and J. A. Yorke, Commun. Math. Phys. **67**, 93 (1979).
[46] S. Succi, Europhys. Lett. **109**, 50001 (2015).
[47] See Supplemental Material at http://link.aps.org/supplemental/10.1103/PhysRevLett.121.236602 for details on the numerical method, which includes Refs. [48–60].
[48] T. Krueger, H. Kusumaatmaja, A. Kuzmin, O. Shardt, G. Silva, and E. Viggen, *The Lattice Boltzmann Method: Principles and Practice* (Springer, New York, 2016).
[49] F. J. Higuera, S. Succi, and R. Benzi, Europhys. Lett. **9**, 345 (1989).
[50] H. Chen, S. Chen, and W. H. Matthaeus, Phys. Rev. A **45**, R5339 (1992).
[51] Y. H. Qian and S. A. Orszag, Europhys. Lett. **21**, 255 (1993).
[52] P. C. Philippi, L. A. Hegele, L. O. E. dos Santos, and R. Surmas, Phys. Rev. E **73**, 056702 (2006).
[53] M. Sbragaglia, R. Benzi, L. Biferale, H. Chen, X. Shan, and S. Succi, J. Fluid Mech. **628**, 299 (2009).

[54] S. S. Chikatamarla and I. V. Karlin, Phys. Rev. E **79**, 046701 (2009).
[55] M. Mendoza, B. M. Boghosian, H. J. Herrmann, and S. Succi, Phys. Rev. Lett. **105**, 014502 (2010).
[56] P. L. Bhatnagar, E. P. Gross, and M. Krook, Phys. Rev. **94**, 511 (1954).
[57] H. Grad, Commun. Pure Appl. Math. **2**, 331 (1949).
[58] H. Grad, Commun. Pure Appl. Math. **2**, 325 (1949).
[59] X. Shan, J. Comput. Sci. **17**, 475 (2016).
[60] A. Scagliarini, L. Biferale, M. Sbragaglia, K. Sugiyama, and F. Toschi, Phys. Fluids **22**, 055101 (2010).
[61] P. L. Bhatnagar, E. P. Gross, and M. Krook, Phys. Rev. Lett. **94**, 511 (1954).
[62] S. Chapman and T. G. Cowling, Am. J. Phys. **30**, 389 (1962).
[63] G. F. Giuliani and G. Vignale, *Quantum Theory of the Electron Liquid* (Cambridge University Press, Cambridge, England, 2005).
[64] S. Succi, *The Lattice Boltzmann Equation: For Complex States of Flowing Matter* (Oxford Scholarship Online, Oxford, 2018).
[65] M. Mendoza, I. Karlin, S. Succi, and H. J. Herrmann, Phys. Rev. D **87**, 065027 (2013).
[66] A. Gabbana, M. Mendoza, S. Succi, and R. Tripiccione, Phys. Rev. E **95**, 053304 (2017).
[67] A. Gabbana, M. Mendoza, S. Succi, and R. Tripiccione, Phys. Rev. E **96**, 023305 (2017).
[68] M. J. M. de Jong and L. W. Molenkamp, Phys. Rev. B **51**, 13389 (1995).
[69] C. Stampfer (private communication).